A study of advection of short wind waves by long waves from surface slope images

X. Zhang, J. Klinke, and B. Jähne
SIO, UCSD, CA 92093-0230, USA

Abstract

Spatial and temporal measurements of short wind waves can be obtained by laser scanning slope gauges and surface slope imaging detectors in the recent development of optical techniques. Slope image data from wind wave experiments in wind wave facilities at Heidelberg and Marseille are used to study the propagation of short wind waves. The data were acquired by an interlaced CCD camera. Each pair of images is consisted of odd and even video fields that are 1/60 second apart. The propagation speed of short wavelets can thus be measured directly through tracking wavelets between a pair of the field images.

The images are filtered into different spatial scales. The pairs of the spatial components are matched up for estimating the propagation speeds of waves at different wavelengths. The shortest waves are parasitic capillaries which are capable of matching the speed of long waves. They are quasi-stationary relative to the crest of the long wave within our measurement accuracy. This suggests that the group velocity of parasitic capillaries must be in near balance with the local orbital velocity of the underlying long wave. The waves of different lengths propagate, on the average, at different speeds proportional to the dispersion relation, and are not locked into the long wave phase speeds. There is a large variation in the propagating speeds due to the orbital advection by long waves.

1 Introduction

It is well known that Bragg scattering from short surface waves is one of the major mechanisms which contributes to radar returns in scattering from rough sea surfaces. It has been suggested that non-Bragg scattering processes due to wave breaking are also present (Trizna et al 1991). The short waves propagate slower than both the long waves and extremely short capillaries. The fast and slow scatterers have been distinguished in measured polarimetric Doppler spectra at small-grazing angle (Lee et al 1996). The early success in, and need for further understanding of, microwave remote sensing ocean surface have stimulated great interests in the study of dynamics of short wind waves.

Short waves riding on long waves are modulated by, and interact with, the long waves (Longuet-Higgins & Stewart 1960, Phillips 1981, Longuet-Higgins 1987, Zhang and Melville 1990). Near the crest of the long waves, short waves are compressed and may break. Very short capillaries, such as parasitic capillaries, are compressed towards long wave troughs (Zhang 1995). Under a two-scale hypothesis, in a frame of moving with a dominant

wave, the measured propagation speed of a short wavelet equals $c-U_c$, where $U_c^2 = C - 2g\eta$. Here C, U_c and η are the phase speed, orbital velocity, and height of the dominant wave, and c is the local phase speed of the short wavelet. The evolution of short wind-generated waves is even more complicated because the waves are also influenced by the combination of wind force, wave-wave resonant interactions, and strong non-linearity.

Based on their observations that phase speeds of frequency components of wind waves do not obey the usual dispersion relation, Lake and Yuen (1978) proposed a nonlinear wind-wave system. Waves can be completely characterized by a single nonlinear wave train having a carrier frequency equal to that of the dominant frequency in the wind-wave spectrum. Temporal wave measurements can be contaminated by frequency shift due to the orbital motions of long waves. It is essential to determine whether the short wind waves are free (dispersive) or bound (non-dispersive).

Spectra of wind waves extend over a wide range of wavelengths, from a millimeter to 10's meters at sea or to a fraction of a meter in laboratory tanks. In the recent development of optical techniques for surface measurements, spatial and temporal measurements of short wind waves can now be obtained by laser scanning slope gauges and surface slope imaging. However, it is still difficult to obtain both the high wavenumber (limited spatial samples by fast laser scanning) and high frequency (limited by frame speed of video imaging) of very short waves. These limitations prevent a reliable spectral analysis of short wave propagation.

A different approach is used here to study the propagation of short wind waves from the slope image data. Slope image data here are from wind wave experiments in wind wave facilities at Heidelberg and Marseille. The data were captured by interlaced CCD cameras and consist of pairs of video fields 1/60 second apart. The propagation speed of short wavelets can thus be measured directly through tracking wavelets between a pair of the field images. The images are filtered into different wavenumber bands. The pairs of spatial components are matched up for estimating the propagation speeds of waves at different scales. The method is similar to Lake and Yuen's (1978) approach in the frequency domain.

2   Slope image data

Two sets of surface slope images used here are from experiments at the large linear facility of the IMST, University of Marseille (France), and the circular facility at the Institute for Environmental Physics, University of Heidelberg (Germany). The wind wave facility at Heidelberg consists of an annular water channel with a width of .3 m, a height of .7 m, and an outer diameter

of 4 m. The water depth was set at .25 m. The IMST facility is about 40 m long. The water section is 2.6 m wide and 1 m deep, and the air section is 3.2 m wide and 1.5 m high. The data were taken at a fetch of 29 m. All the wave images were acquired with Pulnix TM740 CCD cameras. Because of interlaced scanning, a video frame consists of two fields which are exposed consecutively at a 1/60 second interval. The field images were digitized at a resolution of 512 pixels in the alongwing direction and 240 pixels in the crosswind direction. The spatial resolutions are listed as:

Facility	Image size		SpatialResolution		Nyquist Wavenumber	
	x(cm)	y(cm)	dx(cm)	dy(cm)	kx(rad/cm)	ky(rad/cm)
Maeseille	30.9	23.4	0.0604	0.0975	52.05	32.25
Heidelberg	18	14	0.0352	0.0583	89.36	53.89

Table 1 Summary of the image size and the spatial resolution. The alongwind and crosswind directions are denoted with x and y respectively.

The detailed descriptions of the facilities and experiments can be found in Coantic and Bonmarin (1975), and Klinke and Jahne (1992).

3   Data processing method

Slope images are separated into different scales through filtering. The spectral responses of the filters that were applied to the images are shown in Fig. 1, labeled f0, f1, f2, f3, and h4. h4 is a high pass filter separating parasitic capillaries which peaked near 10 rad/cm. The wavenumber of minimum phase speed is about 3.64 rad/cm, which is just about the cutoff of the filter f2. The cutoff of the filter f1 is about 1 rad/cm corresponding to
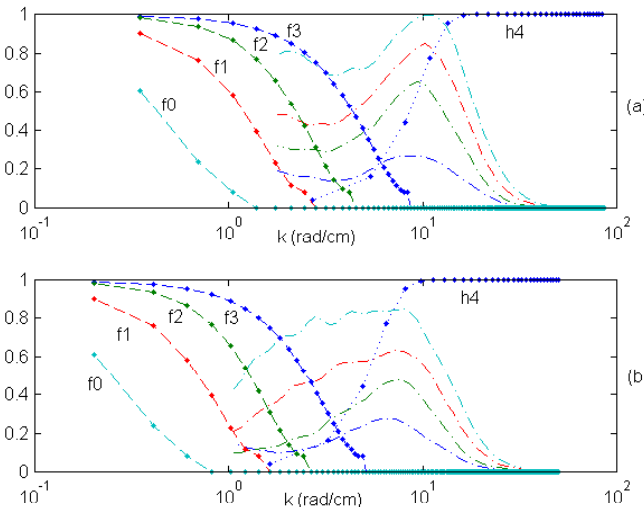

Figure 1. Spectral response of the filters. They are labeled as f0, f1, f2, f3, and h4 respectively. The dot dashed curves are saturation spectra of waves at different wind speeds. The spectra are plotted in log to log and scaled to fit in the plots.(a) the filters for the Heidelberg data, and (b) the filters for the Marseille data.

the 6 cm waves. The low pass filter f0 give the longest wave components. Due to the different spatial sampling rates between the two data sets, the filter cutoffs of the Heidelberg data are shifted up to the higher wave numbers. The five spatial bands of data used here are the outputs from f0, f1-f0, f2-f0, f3-f0, and h4.

The propagation speeds of the spatial components are estimated through cross correlating each pair of spatially filtered slope images. The correlation windows are 128x128, 128x128, 64x64, 64x64, and 32x32 pixels for the corresponding spatial bands. Figure 2 shows examples of even and odd video fields of an alongwind slope image, filtered spatial components, and propagation velocity vectors from matching the even and odd image pairs. The even and odd field images are interpolated according to their true physical aspect ratio (Table 1). The spatial structures of waves are remarkably stable in the 1/60 second between two fields, especially at the small-scale. This allows us to estimate short wave propagation speed from translation of wave spatial patterns. The spatially filtered images are shown (odd field only) together with the estimations of wave propagation speeds respectively. The units given in the vector plots are in pixels, and the vectors are proportional to the pixel translations. In the middle part of lowest frequency image, there is a nearly one-dimensional crest of a dominant long wave. As expected, the slope changes very smoothly at this large scale. However, the smoothness can reduce the accuracy of translation estimations. The estimations around the edges of the image are not reliable because of edge effects normal in spatial filtering. The velocity estimations around the edges of the image are thus ignored in the following results. The velocity vectors are the largest at the lowest spatial mode, and decrease towards the higher spatial modes, in general. For higher frequency components, the propagation speed is higher near the crest of the dominant wave due to the orbital advection. Parasitic capillaries, in the highest frequency band, are intermittent spatially. At low wind speeds, the intermediate wave components are weak and parasitic capillaries are mainly associated with the dominant waves. However, as the wind increases, those intermediate wave components are fully developed and parasitic capillaries appear on wave crests of all spatial components. A threshold (correlation coefficient of 0.6) is applied to velocity vectors of capillaries to eliminate the locations where there is no capillary wave. A median filter was applied to the two-dimensional velocity vector data for reduction of estimation noise.

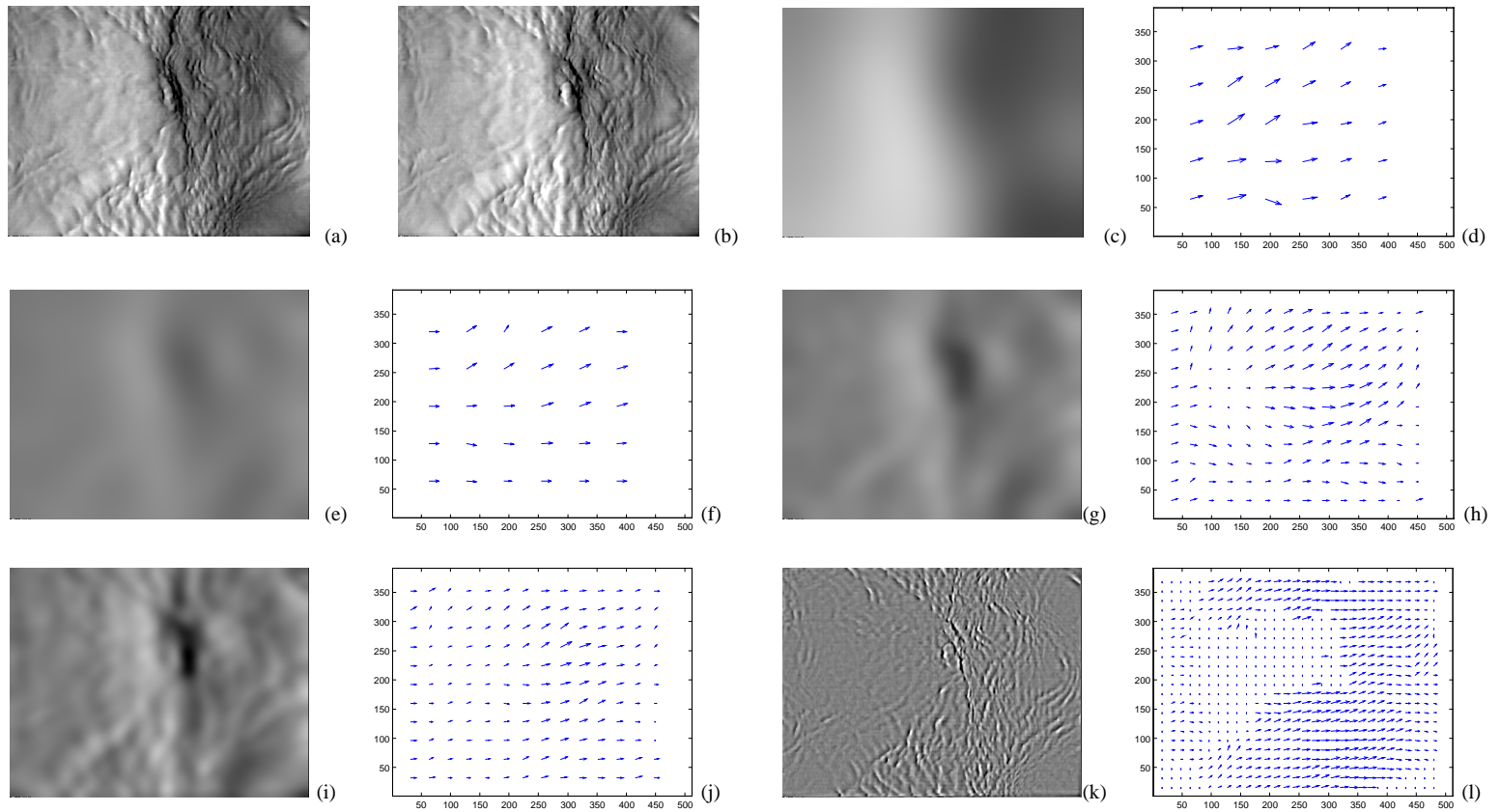## 4   Results and discussions

Figure 2 An example of slope image, filtered wave components, and propagation speeds. (a) and (b) are a pair of even and odd field images. Wind is towards the right at a speed of 8 m/s. (c) and (d) are the lowest wave component and propagation speed vectors. (e) and (f), (g) and (h), (I) and (j), and (k) and (l) are the images of higher wave components and propagation vectors respectively.

The measured wave propagation speed of a free wave equals the phase speed of the short wave plus advection by the orbital velocity of the long waves. The ensemble averaged advection is the residual of orbital motion, Stokes drift, which is about 1% of the wind speed. The propagation speed of high spatial modes would be locked into the speed of the lowest spatial mode if waves were bounded. All images here were acquired at a time interval large enough so that they are statistically unrelated. Figure 3 shows the averaged (over 40 images) propagation speed of waves at different scales, different wind speeds, and two different facilities. The dotted line is the linear phase speed of a free wave. The measurements show here that waves of different scales are dispersive. They propagate at different speeds nearly proportional to the dispersion relation. The velocity distribution averaged within a single image is similar but with a large variation in the off-set from the linear phase
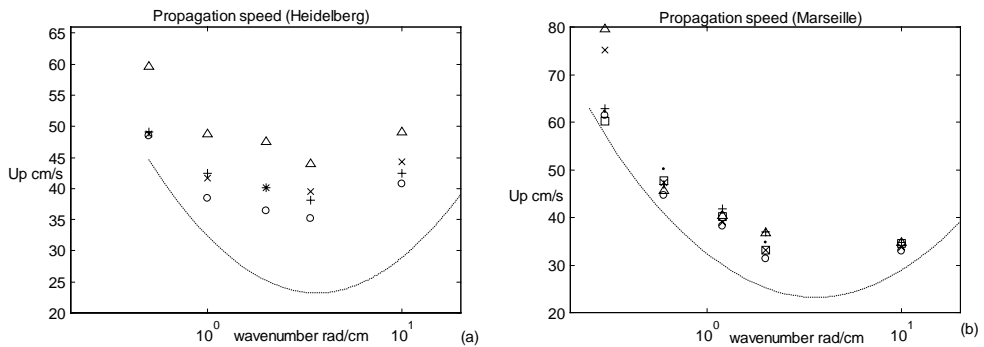

Figure 3 The propagation speeds of different wave components. The dotted curve is the free wave phase speed calculated from linear dispersion relation. (a) Heidelberg data. Wind speeds are 5,6, 8 and 10 m/s noted by +, o, ×, and △ respectively. Each data point is an average over 40 images. (b) Marseille data. Wind speeds are 3, 4, 5, 6, 8, and 10 m/s noted by +, □, o, ×, △, and • respectively.

speed curve. This variation can be attributed to the local orbital advection by dominant long waves at different wave phases.

The advection residual of Heidelberg wave data is much more pronounced than that of Marseille wave data. The measured wind friction velocity of Heidelberg tank is about 1.5 to 2 time larger than that of the Marseille tank. The water depth is only about 25 cm in the Heidelberg tank, comparable to the length of dominant long waves. The long waves can be more nonlinear which generates the stronger drift. The larger wind and wave drift current is contributed to this pronounced advection residaul.

Capillaries are strongly dissipated by viscosity. They cannot last for more than a few wavelengths without constant energy input. Parasitic capillaries propagate, downward from the crest, on the forward face of underlying waves. In order to gain energy from long waves though orbital

compression, their group velocity has to be slightly larger than the orbital velocity, since

$$\partial \ln(k)/\partial U_c = 1/(c_g - U_c)$$

where k and c_g are the wavenumber and group velocity of capillaries, U_c is the orbital velocity in the reference frame of the moving long wave (Zhang 1995). The fractional rate of change in the wavenumber of short waves with respect to the orbital velocity depends on the difference between the group
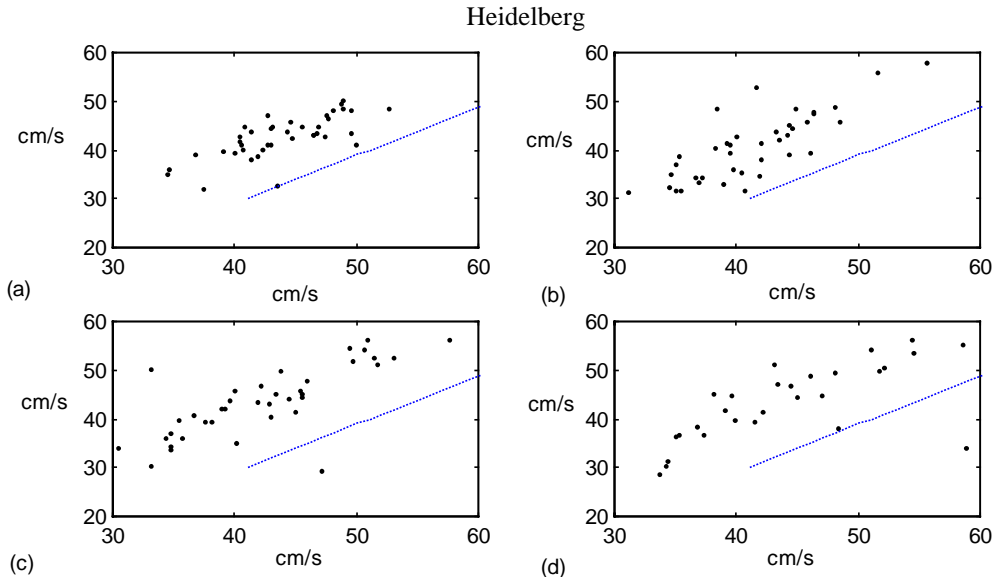
Heidelberg

Figure 4 The propagation speed of capillaries (vertical axis) versus the propagation speed of the carrying waves (horizontal axis). Wind speeds are 5, 6, 8, and 10 m/s in (a), (b), (c), and (d) respectively. The dotted straight line in the plots is C-$(c_g$-c$)_{min}$ versus C.

velocity and the orbital velocity. The measured propagation speed is (c-U_c+C)= (c_g- U_c)+C-(c_g-c). C and c are the phase velocities of the long wave and capillary wave. If (c_g- U_c) is close to zero, the measured speed should be close to C-(c_g-c). Then c and c_g can be estimated from the local wavenumber through the dispersion relation. For a simple estimation, the wavenumber at the peak of parasitic capillaries is used, and thus, the lower bound of (c_g-c)$_{min}$=11.1 cm/s. In Figs. 4 and 5, the measured propagation speed of capillaries is plotted against the averaged propagation speed of all other larger scale waves. The straight line in the plots is C-(c_g-c)$_{min}$ versus C. The data cluster around the predicted straight line for the large linear tank and above the line for the circular tank. This suggests that wind forcing on capillaries may be more important at a long fetch in the large linear facility than the circular tank.

5   Conclusions

Solid evidence is found that short wind waves in the wave facilities are predominately dispersive rather than bounded to the dominant wave components.   The capillaries are closely resonant with the longer wave components. They can extract energy directly from the long waves and may be important dissipation sources of longer wave components especially at low wind speeds.
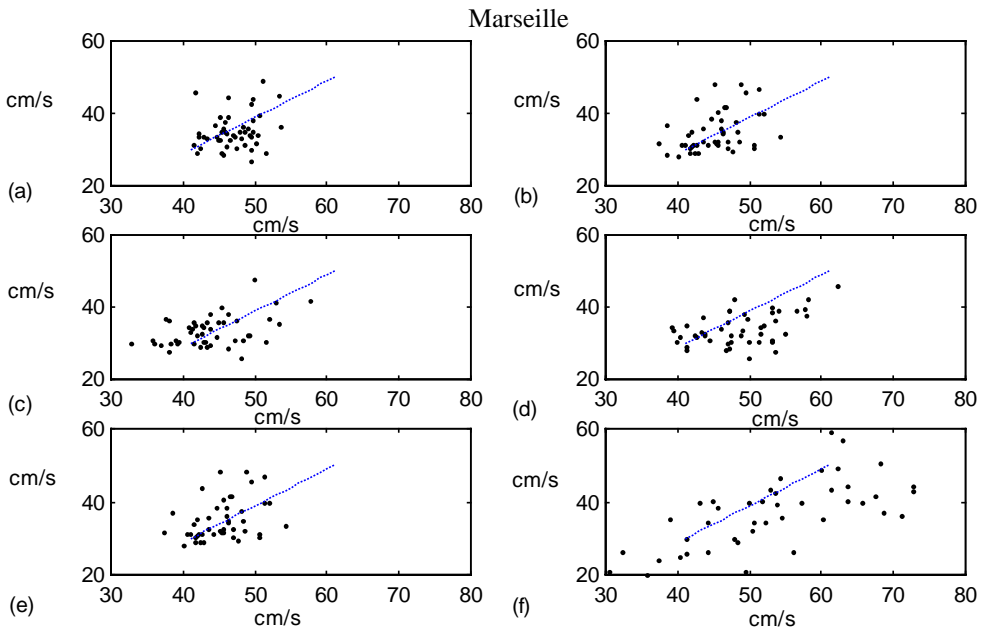

Figure 5 The propagation speed of capillaries versus the propagation speed of the carrying waves. Wind speeds are 3, 4, 5, 6, 8, and 10 m/s in (a), (b), (c), (d), (e), and (f) respectively. The dotted straight line in the plots is $C-(c_g-c)_{min}$ versus C.

References

Coantic, M. and Bonmarin, P. 1975 Atmos. Technol. Vol. 7, 72-79

Klinke, J. and Jähne, B. 1992 SPIE, Vol. 1749, 245-257

Lake, B. M. and Yuen, H. C. 1978 JFM Vol.88 part 1, 33-62

Lee, P. H. Y., Barter, J. D., Caponi, M., Hindman, C. L., Lake, B. M., and Rungaldier, H. 1996 IEEE Trans. Antennas Propag. AP-44, 333-340

Longuet-Higgins, M. S. and Stewart, R. D. 1960 JFM Vol.8, 565-583

Longuet-Higgins, M. S. 1987 JFM Vol. 177, 293-306

Phillips, O. M. 1981 JFM Vol. 107, 465-485

Trizna, D. B. et al 1991 JGR Vol. 96 No. C7 12529-12537

Zhang, J. and Melville, W. K. 1990 JFM Vol. 214, 321-346

Zhang, X. 1995 JFM Vol. 289, 51-82